JMEPEG (2004) 13:735-743
DOI: 10.1361/10599490421565

1059-9495/$19.00

Postprocessing Effect on the Ductility and Flexural Behavior of Three Titanium Alloys Under Simulated Superplastic Forming Conditions

F. Pitt, M. Ramulu, P. Labossiere, and S. Young

(Submitted September 27, 2004)

Ductility of three titanium alloys was evaluated after exposure to time and temperature conditions representative of superplastic forming (SPF). Following exposure, flexural specimens were postprocessed to remove the α-case by one of three methods: no material removed, the standard amount of material removed by chemical processing, or a reduced amount of material removed also by chemical processing. Results include the evaluation of the specimens per ASTM E 290-97a and AMS-T 9046, springback analysis, and prediction of minimum bend radius criteria for the three alloys from finite element method simulation. It was found that results varied based on alloy and exposure temperature and the reduced postprocessing of titanium SPF parts produced acceptable results under certain conditions.

Keywords bending, finite element modeling (FEM), flexure testing, postprocessing, superplastic forming (SPF), titanium (Ti)

1. Introduction

Superplastic forming (SPF) is used to fabricate structural components in multiple industries including the automobile and aircraft industries. Ti-6Al-4V (or Ti-6-4) is the standard SPF titanium alloy in production today. Other titanium alloy candidates for SPF are compared against the properties and performance of Ti-6-4, with regard to advantages in manufacturing, operator safety, reduced maintenance of tooling and forming presses, and longer tool and equipment life. However, other alloys are often processed using the same procedures and requirements currently in place for Ti-6-4 (Ref 1-3), which does not necessarily meet the specific requirements of the other alloy.

All titanium SPF alloys have a tendency to absorb oxygen on any surface exposed to air during the SPF process. This oxygen-rich, contaminated layer, known as alpha case (α-case), is brittle in nature and detrimental to the performance and appearance of the parts (Ref 4). The duration and temperature of exposure have a significant influence on the depth of the oxygen-contaminated layer. The type of alloy also has a significant effect on the amount of absorbed oxygen. Sources show that the depth of increased microhardness due to absorbed oxygen varies depending on alloy and temperature of exposure (Ref 5). It was also found that each SPF alloy has a unique relationship between α-case depth and increased hardness depth and that the microhardness is increased below the depth of visible α-case.

This α-case layer is usually removed from the SPF components by postprocessing using a chemical milling process. However, the chemical milling process is known to cause detrimental effects such as excessive thinning and hydrogen embrittlement. In addition, the chemical operations are hazardous to manufacturing personnel and generate environmentally hazardous waste. If a processing method can be developed to eliminate the need for chemical milling, that is, minimize or eliminate the contaminated layer, the cost and material efficiency of titanium SPF will improve. At the Boeing Company, a growing number of titanium SPF parts are fabricated that use a reduced chemical process and do not go through the standard chemical milling process (Ref 3). This is accomplished by utilizing lower forming temperature alloys, for example, SP 700 and enhanced Ti-6-4, along with extended chemical cleaning. The extended chemical cleaning removes the small amount of contaminated material on the surface.

The α-case layer affects the mechanical properties of the completed parts (Ref 4, 6, 7). In particular, fatigue life is negatively affected. Also, increased oxygen levels are associated with increased microhardness and decreased ductility in titanium (Ref 6). Considerable data exist in the literature regarding Ti-6-4 and the influence of oxygen on mechanical properties. A smaller body of data reflects the influence of oxygen contamination on Ti-6-4 formed at its nominal SPF temperature of 900 °C (1650 °F). The tendency is to assume that other superplastic titanium alloys behave in a similar manner. Indeed, SP 700 and Ti-6Q2 do not behave the same as Ti-6-4 regarding the relationship between increased hardness depth and α-case depth and so should not be expected to behave the same as Ti-6-4 in other instances (Ref 5). Additionally, their optimum SPF temperatures are much lower than that of standard Ti-6-4 (Ref 1).

To date, no data regarding sub-α-case contamination and its

This paper was presented at the International Symposium on Superplasticity and Superplastic Forming, sponsored by the Manufacturing Critical Sector at the ASM International AeroMat 2004 Conference and Exposition, June 8-9, 2004, in Seattle, WA. The symposium was organized by Daniel G. Sanders, The Boeing Company.

F. Pitt, The Boeing Company, Box 3707, Seattle, WA 98124; **M. Ramulu, P. Labossiere,** and **S. Young,** Department of Mechanical Engineering, Box 352600, University of Washington, Seattle WA 98195. Contact e-mail: franna.s.pitt@boeing.com.

influence on mechanical properties of SPF titanium alloys has been available in the literature. Recently, the authors undertook a larger study that addressed the differences in the three aforementioned alloys relative to interstitial (oxygen) contamination during SPF conditions and proposed a more efficient postprocessing method that would result in mechanical properties similar to those obtained with the current postprocessing method. Following SPF, it is usual to post process the material to remove the α-case based on the experimental measurement of α-case depth. As the SPF temperature is reduced, the α-case may not be present, however, the oxygen enrichment in the subsurface material may still be a factor.

The purpose of this paper is to present the effects of differences in alloy composition and postprocessing on the ductility and flexural behavior of three titanium alloys after exposure to SPF conditions. The flexural test as described by ASTM E 290-97a and AMS-T 9046 was conducted on titanium sheet to assess whether the surface and subsurface contaminants have an effect on ductility after postprocessing. The ductility was characterized using bending tests and finite element modeling (FEM), and the results were used to determine whether detrimental contamination exists. In addition, the results of this investigation were used to predict the ratio of minimum successful bend radius to thickness ratio for a variety of conditions and alloys.

2. Experimental Setup and Procedures

2.1 Materials

Three titanium alloys namely, Ti-6Al-4V (Ti-6-4) (Ref 8), Ti-6Al-2Sn-2Zr-2Mo-2Cr (Ti-6Q2) (Ref 9), and Ti-4.5Al-3V-2Fe-2Mo (SP 700) (Ref 10), in sheet form were used in this investigation. Room-temperature mechanical properties of the three alloys are listed in Table 1.

2.2 Experimental Procedure

The bend test specimens were fabricated by machining to dimensions of 203 × 25.4 × 1.5 mm (8 × 1 × 0.06 in.). The fabricated specimens were tagged and chemically cleaned. Specimens were grouped by exposure temperature: 788 °C (1450 °F), 845 °C (1550 °F), and 885 °C (1625 °F). They were conditioned in elevated-temperature air for 90 min, representing the maximum time for superplastically formed airplane components. Individual specimens were hung by stainless steel wire on a rack. Each group was exposed in an air furnace at the appropriate temperature, then unloaded and allowed to cool in room air. Exposed specimens were sectioned, mounted, polished, and then etched with ammonium bifluoride for metallurgical examination.

Three postprocessing conditions explored in this investigation included as-exposed (no additional processing), minimal material removal (α-case plus an amount equivalent to that removed during routine cleaning), and the traditional process (material removed to 150% of the measured depth of α-case). These conditions were compared with the two control groups: as-received material and material that has been subjected only to chemical milling. The process designations are shown in Table 2.

Table 1 Mechanical properties of subject titanium alloys

Alloy	TYS, MPa (ksi)	UTS, MPa (ksi)	*E*, GPa (msi)	*e*, %
Ti-6-4	1094 (158.7)	1108 (160.7)	128 (18.6)	15.8
Ti-6Q2	1115 (161.7)	1156 (167.7)	126 (18.3)	13.3
SP 700	1085 (157.4)	1087 (157.7)	120 (17.4)	13.0

TYS, tensile yield stress; UTS, ultimate tensile strength; *E*, modulus of elasticity; *e*, elongation

Table 2 Process designations

As-received	Chemically milled	As exposed	Proposed process	Current process
AR (control)	CM (control)	AE	PP	FP

Table 3 Test matrix

Number of specimens	Exposure temperature	AR	CM	AE	PP	FP
Ti-6-4	None	3	3	…	…	…
	788 °C (1450 °F)	…	…	3	3	3
	845 °C (1550 °F)	…	…	4	4	4
	885 °C (1625 °F)	…	…	4	4	4
SP 700	None	3	3	…	…	…
	788 °C (1450 °F)	…	…	3	3	3
	845 °C (1550 °F)	…	…	4	4	4
	885 °C (1625 °F)	…	…	4	4	4
Ti-6Q2	None	3	3	…	…	…
	788 °C (1450 °F)	…	…	3	3	3
	845 °C (1550 °F)	…	…	4	4	4
	885 °C (1625 °F)	…	…	4	4	4

Thus, the test matrix consisted of three titanium alloys, exposed to a simulated SPF cycle at three different temperatures and subjected to three different processes after exposure. The test matrix is shown in Table 3.

The specimens were divided into five exposure groups. The as-received (AR) group was tested without further processing. The chemically milled (CM) group was chemically milled to remove 0.127 mm (0.005 in.) of material from all surfaces prior to testing. The proposed process (PP) group was first abraded, and then chemically cleaned three times per the Boeing specification for cleaning titanium, representing the minimum number of cleaning cycles seen by SPF components (average 0.038 mm, or 0.0015 in., of material removed). The current process (FP) group was abraded to remove the scale, then chemically cleaned and further chemically milled to remove the greater of 0.127 mm (0.005 in.) or 150% of the measured α-case from all surfaces of the material, similar to the current standard process for removal of α-case on SPF components.

2.3 Bend Tests

Bend tests were conducted according to ASTM E 290-97a and AMS-T 9046 specifications with the exception of the requirements for a passing result. The criterion for this investigation was chosen based on actual results from the as-received specimens and was determined from the minimum radius to thickness ratio (*R*/*t*) that produced no cracking in the

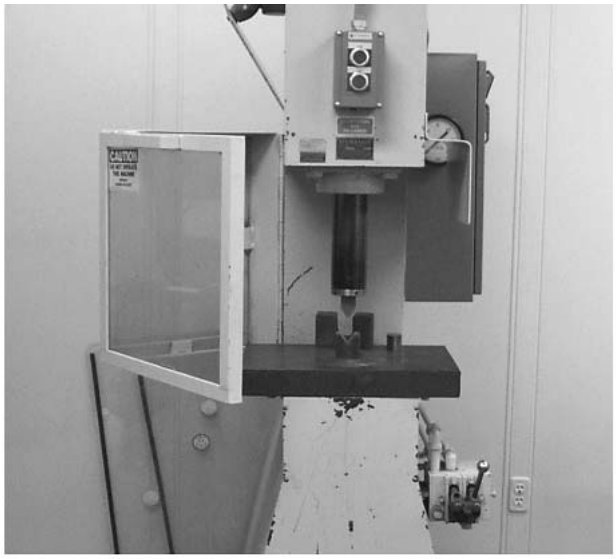

(a)

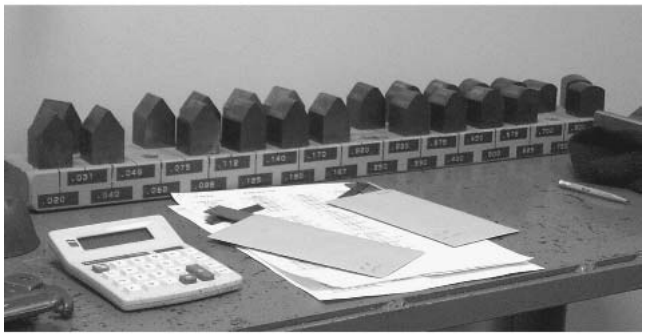

(b)

Fig. 1 (a) Flexural bend test machine and (b) array of different sized punches

as-received material of each of the three alloys. Based on the results of bending the AR specimens, *R*/*t* of 3.0 became the standard to discriminate between passing and failing results. This ratio is more severe than the requirement in the material specifications, which is *R*/*t* of 9.0 for SP 700 and Ti-6Q2 and *R*/*t* of 4.5 for Ti-6-4. Based on the specimen thickness, the appropriate die is selected from a set of dies to give an *R*/*t* as close as possible to the target. The actual *R*/*t* is recorded based on the actual specimen thickness and die radius (Ref 8-10).

To accomplish the test, the die punch is loaded into an automated press and centered over the die tup as shown in Fig. 1(a). The set of die tups used in this investigation is shown in Fig. 1(b). The rectangular specimen is placed on the tup and the punch is activated. It moves vertically into the tup, bending the specimen into the tup. After bending, the specimen is viewed at a magnification of 20×. The outer bend surface is examined for cracks and crack indications. If there are no cracks or indications of possible cracks, the specimen passes the test. Otherwise it fails. Specimens are bent from both sides, checking each surface in tension. Each specimen can produce several bends along its length. A total of 371 bending tests were conducted in this investigation.

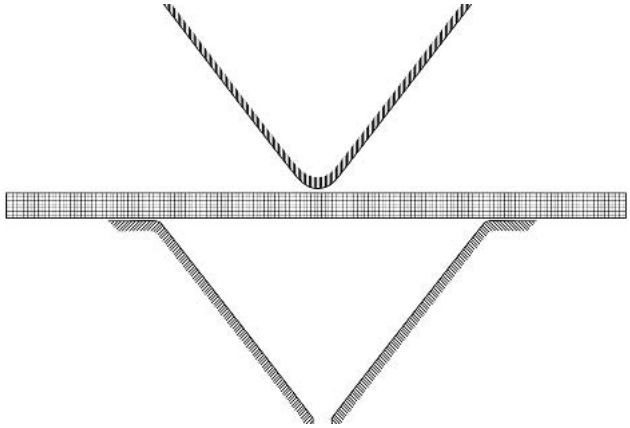

Fig. 2 Schematic illustration of the numerical simulation model of the flexural test of the titanium alloy sheet showing representative FEA mesh

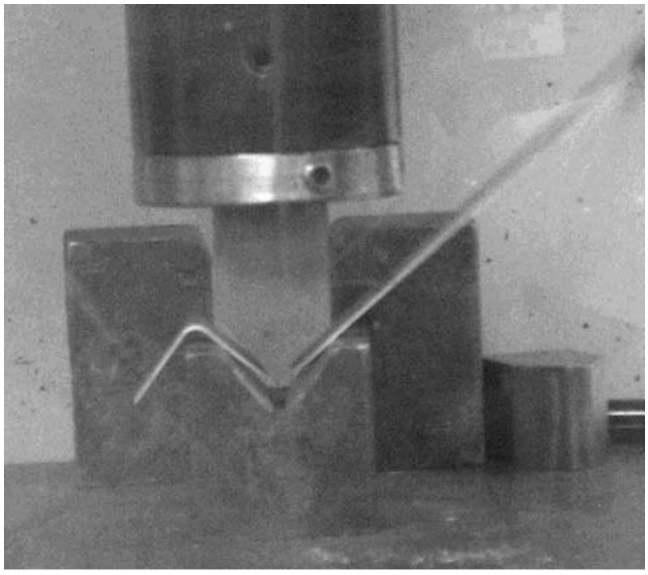

(a)

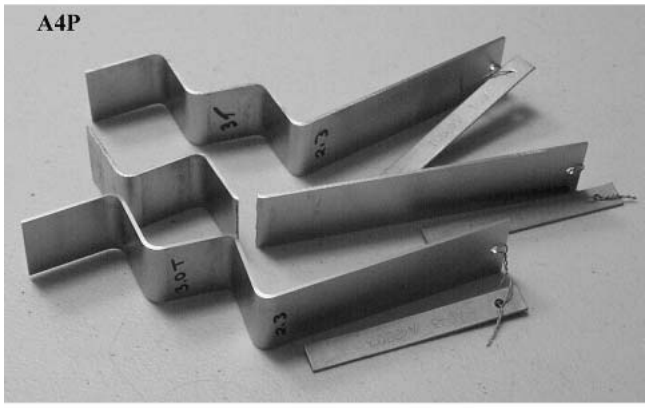

(b)

Fig. 3 Typical specimen under bend cycle and tested specimens. (a) Flexural specimen during second bend cycle. (b) Tested specimens

Sheet bend data consist of the specimen thickness, radius of the bending tup, the final relaxed angle of each bend, and whether cracks are present in the radius area of the specimen. Specimens were manually measured using a digital micrometer and manually recorded. Sizes of the bending tups were manually recorded. After testing, the specimens were examined visually under a 20× lens, and if cracks were present, this was also recorded manually. The bend angle was measured using an adjustable protractor. Each condition contained three specimens, and each specimen contained multiple bends. If any of the bends on any of the specimens exhibited cracking, the condition was marked as failed.

2.4 Finite Element Model

Finite element analysis (FEA) was used to predict the internal stress distribution and deformation upon loading and unloading of the titanium sheets during flexural testing. The nonlinear analyses were done using the commercial code ANSYS (ANSYS, Inc. Southpointe, Canonsburg, PA). FEA models took advantage of symmetry and were based on plane strain assumptions since the model is relatively thick in the through thickness direction. Initial three-dimensional (3-D) models showed that the difference in accuracy between the two-dimensional (2-D) and 3-D solutions was minimal. Typical models consisted of ~1800 degrees of freedom. A representative FEA mesh is shown in Fig. 2. The mesh included the model representation of the die punch and die tup. The die punch and die tup were modeled with analytical rigid surfaces, and the contact interaction pairs were defined between these and the deformable FEA mesh of the sheet. A coefficient of friction of 0.2 was assumed between the contact pairs, and it was noted that, although the internal stress distribution was somewhat influenced by this choice, the effect on

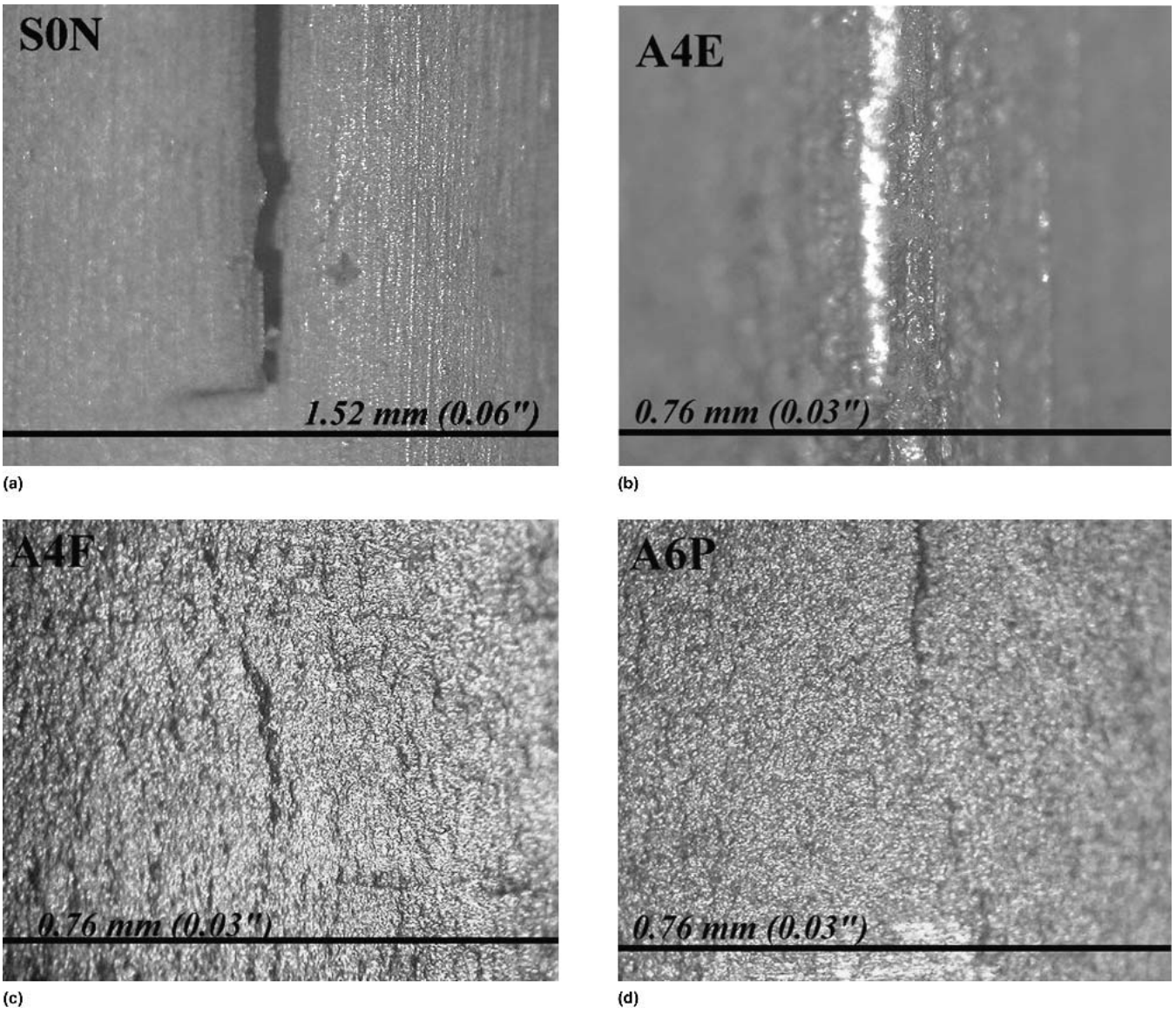

Fig. 4 Typical cracking and failure in SPF specimens after bend test. (a) AR. (b) AE. (c) FP. and (d) PP

the overall behavior was minimal over a reasonable range of coefficients of friction. The material property measurements reported in Ref 11 were implemented within the bilinear isotropic hardening plasticity subroutine within ANSYS. A model was generated for each sheet material and die punch geometry combination. Loading was applied by prescribing a vertical displacement to the rigid surface representing the die punch while the displacement of the rigid surface representing the die tup was held fixed.

3. Results and Discussion

The ductility and flexural behavior of three titanium alloys were compared after exposure to simulated SPF conditions at 788 °C (1450 °F), 845 °C (1550 °F), and 885 °C (1625 °F) for 90 min. Figure 3 shows a typical specimen in the process of being bent for a second time in the opposite direction of the first bend. Notice that each specimen is bent multiple times and thus yields more than one data point. Success in bending was evaluated with pass (no cracking) and fail (cracking and/or fracture) criteria. Typical samples of failed bend surfaces are shown in Fig. 4.

Ductility was characterized in terms of the minimum ratio of bend radius (R) to thickness (t) of the sheet (R/t), and whether surface cracking on the tension side of the bent surface was present. The springback angle α (i.e., the included bend angle) was used to characterize the flexural behavior for the corresponding minimum bend radius (R/t). Tables 4 and 5 list the experimentally evaluated bend radii and R/t ratios for passing and failing conditions, respectively. Figures 5(a) to (c) show graphically the pass/fail results for each alloy compared with the bend angles after springback and the R/t ratio of the individual bend. Each of the processing conditions is identified with a different symbol on these three graphs. Notice that the flexure failure clearly depends on the alloy type and the processing condition. The results, when compared, seem to fall into three categories:

- Failed specimens with large bend angles (α), often completely fractured
- Failed specimens with generally smaller bend angles (α) than the passing specimens
- Passing specimens within a fairly small range of bend angles (α)

The data represent five different processing conditions including as-received, chemically milled, as exposed to simulated SPF conditions, postexposure processed with the proposed reduced method, and postexposure processed with the full existing production process. The differences in bend angles and the minimum bend radius (R/t) are apparent between alloys and the different processing conditions. The average minimum R/t ratio for successful bending for Ti-6-4, Ti-6Q2, and SP 700 was in the range of 2.5 to 3.4, 2.2 to 3.5, and 2.3 to 5.0, respectively, as shown in Table 4. The associated average post to bend angles (α) of the passing specimens were in the range of 88 to 99° for all the processing conditions considered in this investigation. Regardless of exposure temperature, the as-exposed specimens of each alloy resulted in failed bends (Table 5). Also, notice that the final angle of the failed specimens (α) was in the range of 81 to 163°. Figures 6(a) to (c) show the passing percentages for each alloy compared with the R/t = 3.0 passing standard set by the as-received material.

The screening test method of ASTM E 290-97a with R/t

Table 4 Minimum bend (R/t) ratios and resting angles associated with pass condition

Process	Material	Temperature	No. of bends	R/t	Angle	Thickness, mm
AR	Ti-6Al-4V	N/A	7	3.174 ± 0.027	88.4 ± 1.4	1.497 ± 0.013
	Ti-6Q2	N/A	11	3.177 ± 0.290	90.5 ± 2.7	1.495 ± 0.005
	SP 700	N/A	12	3.254 ± 0.307	90.9 ± 2.4	1.460 ± 0.031
CM	Ti-6Al-4V	N/A	6	3.175 ± 0.022	87.8 ± 4.2	1.280 ± 0.010
	Ti-6Q2	N/A	6	3.467 ± 0.023	87.2 ± 3.1	1.370 ± 0.010
	SP 700	N/A	12	2.834 ± 0.318	89.9 ± 7.1	1.255 ± 0.009
AE	Ti-6-4	All	0	N/A	N/A	N/A
	Ti-6Q2	All	0	N/A	N/A	N/A
	SP 700	All	0	N/A	N/A	N/A
FP	Ti-6-4	788 °C (1450 °F)	10	2.509 ± 0.334	89.4 ± 8.8	1.228 ± 0.028
		845 °C (1550 °F)	8	3.285 ± 0.040	89.3 ± 6.6	1.083 ± 0.013
		885 °C (1625 °F)	10	2.969 ± 0.488	91.0 ± 5.8	1.103 ± 0.010
	Ti-6Q2	788 °C (1450 °F)	13	2.524 ± 0.357	95.2 ± 10.6	0.989 ± 0.070
		845 °C (1550 °F)	8	2.648 ± 0.082	89.1 ± 3.9	1.200 ± 0.037
		885 °C (1625 °F)	8	2.198 ± 0.100	90.8 ± 5.7	1.111 ± 0.0527
	SP 700	788 °C (1450 °F)	15	2.267 ± 0.107	91.3 ± 8.9	1.257 ± 0.058
		845 °C (1550 °F)	8	3.127 ± 0.134	89.1 ± 3.9	1.139 ± 0.049
		885 °C (1625 °F)	2	5.034 ± 0.000	98.0 ± 2.8	1.119 ± 0.017
PP	Ti-6-4	788 °C (1450 °F)	6	2.956 ± 0.026	90.8 ± 4.5	1.375 ± 0.013
		845 °C (1550 °F)	8	3.094 ± 0.048	89.6 ± 5.0	1.314 ± 0.021
		885 °C (1625 °F)	7	3.406 ± 0.263	90.7 ± 1.3	1.330 ± 0.014
	Ti-6Q2	788 °C (1450 °F)	5	3.399 ± 0.531	92.6 ± 3.8	1.402 ± 0.014
		845 °C (1550 °F)	16	2.530 ± 0.022	99.1 ± 7.9	0.964 ± 0.009
		885 °C (1625 °F)	8	3.064 ± 0.068	97.6 ± 4.9	0.796 ± 0.018
	SP 700	788 °C (1450 °F)	12	2.334 ± 0.090	92.3 ± 5.8	1.362 ± 0.053
		845 °C (1550 °F)	8	3.589 ± 0.068	95.6 ± 5.3	0.885 ± 0.017
		885 °C (1625 °F)	1	3.373 ± 0.000	98.0 ± 0.0	1.243 ± 0.038

ratios from the relevant material specifications is not sufficient to discriminate between the different processing conditions with the possible exception of the as-exposed material, complete with scale, α-case, and increased interstitial oxygen. Some differences are seen when the threshold radius to thickness ratio is determined by the minimum successful *R*/*t* using as-received material (i.e., 3.0 in this study). In this case, the proposed minimum processing following simulated SPF exposure does not always meet the standard set by the as-received material. The high-temperature exposure of SP 700 is one example where the minimum passing *R*/*t* ratio is higher (worse) than in the fully processed condition. However, the 885 °C (1625 °F) temperature is very close to the β transus temperature of this alloy (900 °C, or 1650 °F), and the microstructure is significantly changed to a much higher percentage of β in this case than after exposure to the lower temperatures or in the other two alloys. The higher percentage of β might cause the decreased ductility. More likely, there is increased oxygen diffusion, made possible by the higher diffusion capability of the β microstructure compared with the α microstructure.

Figures 7(a) and (b) show representative plots of the numerical solution for the displaced configuration at full loading, and upon unloading, respectively, in Ti-6Al-4V alloy. The FEA models predict obvious springback upon removal of the die punch that is evidenced by a change in angle upon die punch removal. Figures 8(a) and (b) show magnified views of contour plots of representative axial stress distributions in MPa (stress in the horizontal direction of the undeformed configuration) at full loading, and upon unloading, respectively. The largest stresses occur in the vicinity of the bend as can be seen in Fig. 8(a) at full loading. The maximum stress (σ_{max}/σ_{ys}) was in the range of 1.17 to 1.21 when the finite element method (FEM) was implemented for the five conditions, taking into account their mechanical properties. The model shows that roughly two-thirds of the sheet in the through-thickness direction experiences stresses above the initial yield stress of the material. Upon unloading (die punch removal), the internal stresses remain in the sheet due to irreversible plastic deformation of the sheet. The residual stresses can be seen in Fig. 9. Both the die punch force and the maximum axial stress versus normalized die punch displacement are shown. The force increases linearly upon initial displacement of the die punch, but quickly becomes nonlinear as the deformation becomes plastic. Nearing the end of the die punch displacement, the force begins to rise quickly as the sheet becomes pinched between the die punch and die tup. Similar observations were made by others (Ref 11).

A parametric FEM analysis was conducted to study the bend angle after springback, for varying punch radii (1.9-6.4 mm) for a given die width, material, and its processing condition. Figures 10(a) and (b) show bend radius *R*/*t* versus computed bend angle after springback and the die punch force versus *R*/*t* for various radii *R*, respectively. The solid lines in the graph denote least squares fit to the results including the

Table 5 Maximum bend (*R*/*t*) ratios and resting angles associated with fail condition

Process	Material	Temperature	No. of bends	*R*/*t*	Angle	Thickness, mm
AR	Ti-6Al-4V	N/A	1	2.691 ± 0.000	89.0 ± 0.0	1.497 ± 0.013
	Ti-6Q2	N/A	2	2.942 ± 0.317	126.5 ± 10.6	1.495 ± 0.005
	SP 700	N/A	1	2.832 ± 0.000	89.0 ± 0.0	1.460 ± 0.031
CM	Ti-6Al-4V	N/A	0	N/A	N/A	1.280 ± 0.010
	Ti-6Q2	N/A	0	N/A	N/A	1.370 ± 0.010
	SP 700	N/A	0	N/A	N/A	1.255 ± 0.009
AE	Ti-6-4	788 °C (1450 °F)	6	1.528 ± 0.071	110.8 ± 18.4	1.528 ± 0.029
		845 °C (1550 °F)	8	3.783 ± 0.060	137.3 ± 6.1	1.478 ± 0.024
		885 °C (1625 °F)	8	3.748 ± 0.048	Undetermined	1.491 ± 0.019
	Ti-6Q2	788 °C (1450 °F)	3	1.523 ± 0.064	149.7 ± 7.5	1.523 ± 0.024
		845 °C (1550 °F)	4	4.220 ± 0.067	162.5 ± 5.1	1.505 ± 0.023
		885 °C (1625 °F)	4	4.227 ± 0.058	Undetermined	1.503 ± 0.021
	SP 700	788 °C (1450 °F)	6	1.495 ± 0.043	89.8 ± 0.4	1.495 ± 0.017
		845 °C (1550 °F)	4	3.841 ± 0.122	143.3 ± 4.3	1.463 ± 0.046
		885 °C (1625 °F)	4	3.843 ± 0.171	Undetermined	1.456 ± 0.063
FP	Ti-6-4	788 °C (1450 °F)	5	2.204 ± 0.151	83.0 ± 13.5	1.228 ± 0.028
		845 °C (1550 °F)	0	N/A	N/A	1.083 ± 0.013
		885 °C (1625 °F)	6	2.203 ± 0.015	87.5 ± 9.7	1.103 ± 0.010
	Ti-6Q2	788 °C (1450 °F)	2	2.169 ± 0.163	83.0 ± 0.0	0.989 ± 0.070
		845 °C (1550 °F)	5	N/A	N/A	1.200 ± 0.037
		885 °C (1625 °F)	4	1.717 ± 0.078	81.3 ± 1.9	1.111 ± 0.0527
	SP 700	788 °C (1450 °F)	0	N/A	N/A	1.257 ± 0.058
		845 °C (1550 °F)	12	N/A	N/A	1.139 ± 0.049
		885 °C (1625 °F)	7	4.538 ± 0.893	124.9 ± 14.8	1.119 ± 0.017
PP	Ti-6-4	788 °C (1450 °F)	5	2.309 ± 0.022	90.8 ± 12.8	1.375 ± 0.013
		845 °C (1550 °F)	0	N/A	N/A	1.314 ± 0.021
		885 °C (1625 °F)	9	3.211 ± 0.289	101.9 ± 17.4	1.330 ± 0.014
	Ti-6Q2	788 °C (1450 °F)	1	3.369 ± 0.000	106.0 ± 0.0	1.402 ± 0.014
		845 °C (1550 °F)	0	N/A	N/A	0.964 ± 0.009
		885 °C (1625 °F)	8	2.393 ± 0.053	84.6 ± 6.3	0.796 ± 0.018
	SP 700	788 °C (1450 °F)	0	N/A	N/A	1.362 ± 0.053
		845 °C (1550 °F)	0	N/A	N/A	0.885 ± 0.017
		885 °C (1625 °F)	12	3.741 ± 0.261	125.2 ± 24.5	1.243 ± 0.038

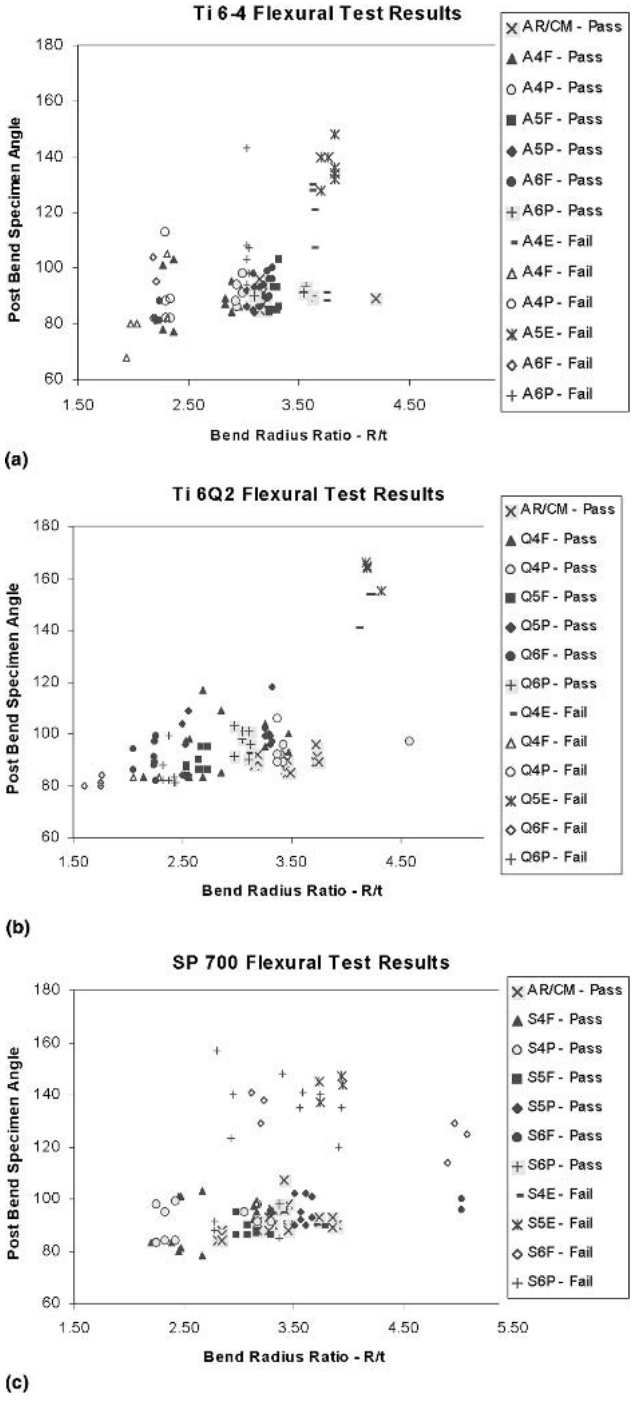

Fig. 5 Postbend specimen angle versus bend radius (*R*/*t*). Solid and shaded symbols indicate passing results for (a) Ti6-4, (b) Ti6Q2, and (c) SP700.

corresponding equations for each fit. As expected, the springback bend angles increased with decreasing *R*/*t* because the thickness increases. Similar observations can be found with the die punch force for varying radii *R*.

Four different process conditions (AR, CM, FP, and PP) of Ti-6Al-4V, FEM simulation experiments were conducted and the parametric results were analyzed. The maximum strain ($\varepsilon_{max}/\varepsilon_{yield}$) was found to be in the range of 1.18 to 1.20 for

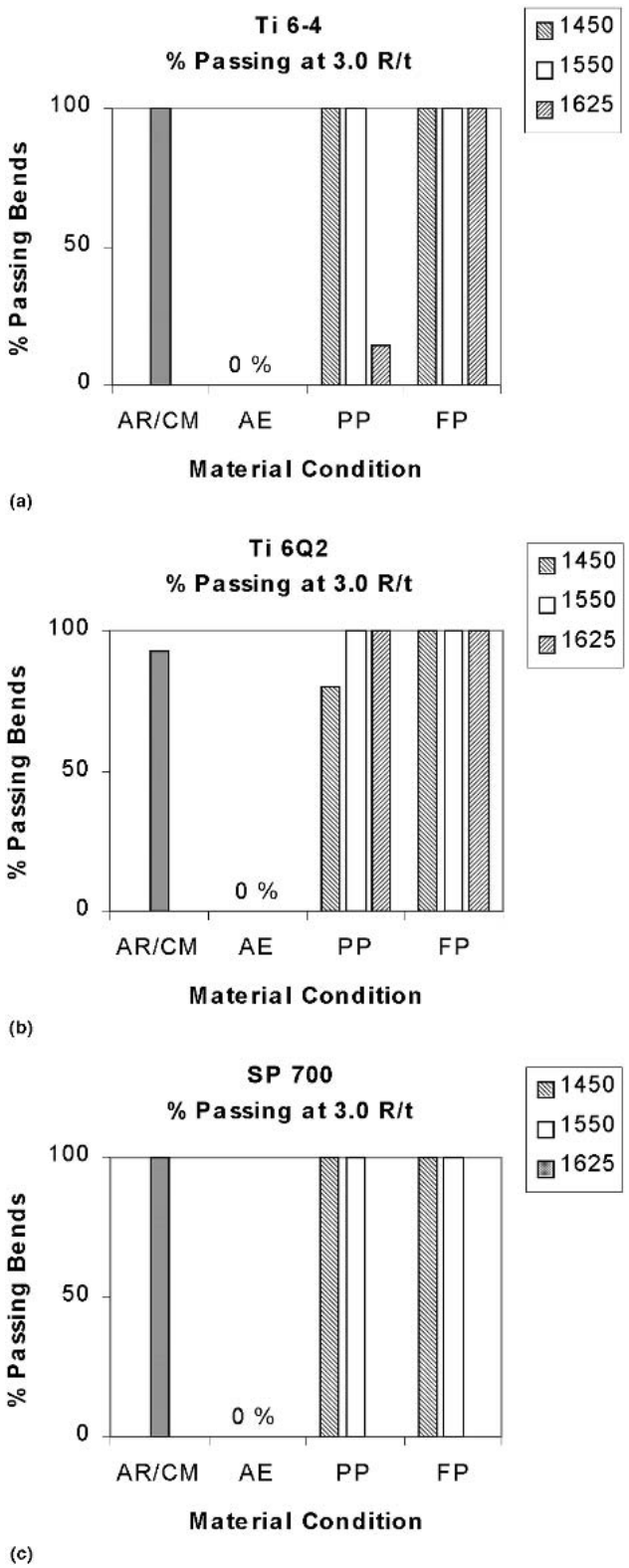

Fig. 6 Percentage passing bends at 3.0 *R*/*t* for (a) Ti6-4, (b) Ti6Q2, and (c) SP700.

successful bending without surface cracking. Based on analysis, a simple power law model was developed for Ti-6Al-4V, relating the bend angle after springback to bend radius *R*/*t*:

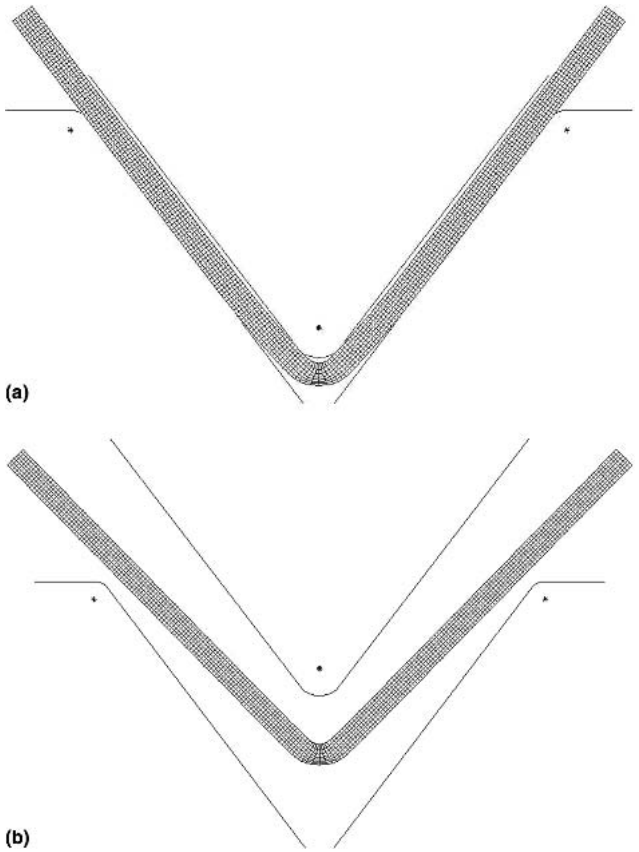

Fig. 7 Representative deformed mesh of the titanium alloy sheet during the flexural test at (a) loading and (b) unloading

$$\alpha = 93\left(\frac{R}{t}\right)^{-0.086} \quad \text{(Eq 1)}$$

Interestingly, the exponent is almost equivalent to half the ultimate strain obtained from tension test results of the Ti-6Al-4V material. Using this equation, springback angles were predicted. The predicted and measured variations in the resting bend angle for varying *R*/*t* ratios and Ti-6Al-4V alloy under all processing conditions are shown in Table 6. The predicted bend angles were smaller than the experimentally measured bend angles. The correlation between measured and predicted bend angles was within 8%. This minor difference could be due to the inaccuracies in experimental measurements as well as simplified assumptions made in FEM modeling.

The experimental results listed in Tables 4 and 5 indicate that the exposure temperature significantly influences the propensity for failure. All of the specimens exposed at the highest temperature (885 °C, or 1625 °F) and postprocessed with the proposed process failed to meet the 3.0 *R*/*t* criterion. In addition, the SP 700 specimens exposed at the highest temperature and postprocessed using the existing process, also failed. These failures also corresponded in part with an increase in the bend radius and larger bend angles. The FEA results show that an increase in the bend radius is consistent with a decrease in the angle as can be seen in Fig. 10(a). This also corresponds to an increase in the maximum strain where the maximum strain is proportional to the thickness of the specimen and inversely

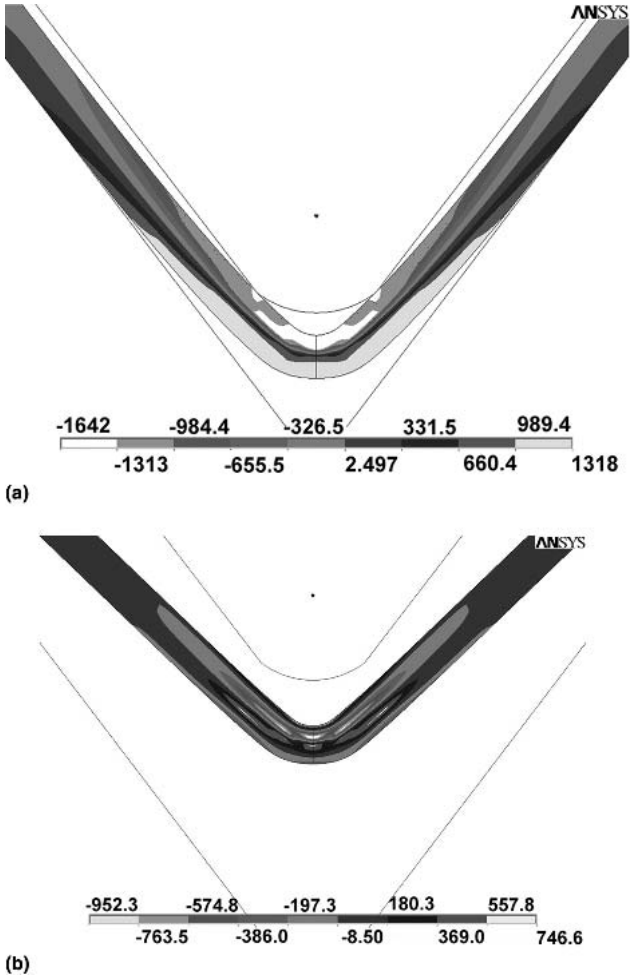

Fig. 8 Magnified view of contour plots of representative axial stress distributions (in MPa) in the titanium alloy sheet during the flexural test at (a) loading and (b) unloading.

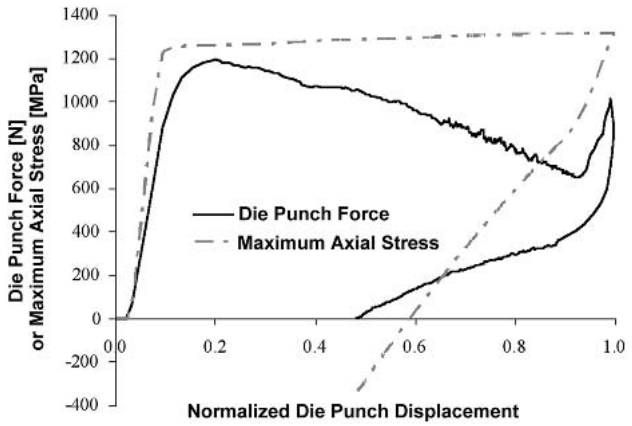

Fig. 9 Representative die punch force (*N*) and maximum axial stress (MPa) in the titanium alloy sheet as a function of normalized die punch displacement

proportional to the bend radius. Thus, failure is more likely to occur when the specimen experiences a higher maximum strain. Depending on the material, this may or may not corre-

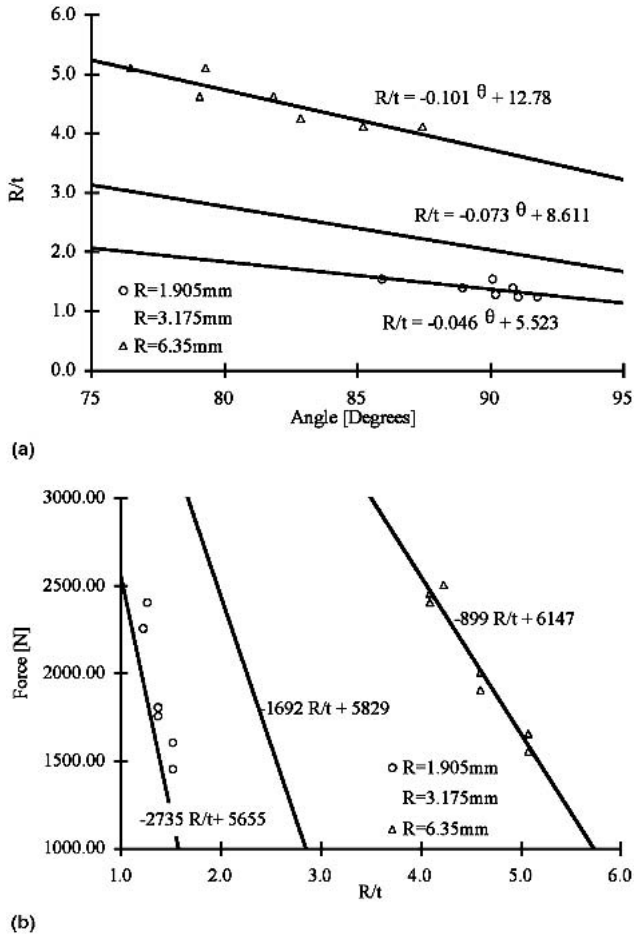

Fig. 10 Die punch force, resting angle versus *R/t* for various punch die radii *R* (the solid lines denote least squares fits to the results). (a) bend radius (*R/t*) versus resting angle α and (b) die punch force versus bend ratio *R/t*

Table 6 Experimental and predicted bend angles in Ti-6Al-4V after springback

Ti-6Al-4V	*R/t*	Experiment	FEM predictions
CM	3.175	87.8	85.4
AR	3.174	88.4	83.9
788 °C (1450 °F), FP	2.509	89.4	86.3
788 °C (1450 °F), PP	2.956	90.8	85.1
845 °C (1550 °F), FP	3.285	89.3	86.2
845 °C (1550 °F), PP	3.094	89.6	84.4
885 °C (1625 °F), FP	2.969	91.0	85.8
885 °C (1625 °F), PP	3.406	90.7	83.2

spond to an increase in the maximum stress in the specimen. The maximum strain occurs at the outer surfaces of the specimen, whereas the maximum stress occurs somewhere inside the specimen as determined by FEA and shown in Fig. 8(a) of the stress contours in the deformed configuration.

The methodology developed in this study to determine the best bend angle for a given alloy and condition can be extended to additional alloys.

4. Conclusions

The ductility of three titanium alloys was evaluated after exposure to time and temperature conditions representative of SPF. The Ti-6Q2 and SP 700 alloys respond differently than the standard alloy Ti-6Al-4V to SPF conditions and postprocessing operations. Based on the experimental and numerical analysis of flexural results the following conclusions were derived:

- The flexural method investigated herein can be used as a rough screening method for determining the presence of a brittle surface condition due to α-case or increased sub-α-case oxygen when the minimum threshold *R/t* is determined by the as-received material. The method does not appear to be sensitive enough to replace the current method of using light microscopy on polished cross-section material to verify presence or absence of α-case.
- The proposed reduced processing method appears to produce successful flexural properties in all three alloys exposed at the lowest and intermediate temperatures (788 °C, or 1450 °F) and (845 °C, or 1550 °F), which are the best candidate temperatures for increasing the efficiency of the SPF process.
- The proposed process is less successful at the highest exposure temperature (885 °C, or 1625 °F) for Ti-6-4 and SP 700, although the change in microstructure of the SP 700 is the most likely cause of the failures in that material.
- The FEM predicted bend angles after springback were within 8% of the experimentally measured bend angles for a given bend radius (*R/t*) in the Ti-6Al-4V alloy.

References

1. R.J. Tisler and R.J. Lederich, Advanced Superplastic Titanium Alloys, *Titanium '95 Science and Technology, Proceedings of the Eight World Conference on Titanium,* P.A. Blenkinsop, W.J. Evans, H.M. Flowers, Ed., The Institute of Materials, 1995, p 596-603
2. W.D. Brewer, R.K. Bird, and T.A. Wallace, Titanium Alloys and Processing for High Speed Aircraft, *Mater. Sci. Eng.,* Vol A243, 1998, p 299-304
3. P.N. Comley, Aerospace Part Production Using SP700, *Mater. Sci. Forum,* Vol 357-359, 2001, p 41-46
4. F. Pitt, "Influence of Time, Temperature and Alloy on Oxygen Absorption in SPF Titanium," University of Washington, 2000
5. L.J.H. Brasche and O. Buck, Nondestructive Methods for Determination of Mechanical Properties of Aluminum and Titanium Alloys, *Review of Progress in Quantitative Nondestructive Evaluation,* Vol 10B, D.O. Thompson and D.E. Chimenti, Ed., Plenum Press, 1991, p 1701-1706
6. A.I. Kahveci and G.E. Welsch, Hardness versus Strength Correlation for Oxygen-Strengthened Ti-6Al-4V Alloy, *Scr. Metall. Mater.,* Vol 25, 1991, p 1957-1962
7. R.J. Tisler, "Advanced Superplastic Titanium Alloys," presented at the Annual Corporate Technology Conference Advanced Materials & Structures Technology Session, McDonnell Douglas Aerospace (Long Beach, CA), May 18, 1995
8. "Ti-6Al-4V Material Specification," AMS-T-9046, AB-1, Society of Automotive Engineers, 1999
9. "Ti 6-2-2-2-2 Material Specification," AMS 4898, Titanium Alloy, Sheet, 6Al-2Sn-2Zr-2Mo-2Cr-0.15Si, Annealed, Society of Automotive Engineers, 1996
10. "SP 700 Material Specification," AMS 4899, Titanium Alloy, Sheet, Strip, and Plate, 4.5Al-3V-2Fe-2Mo, Annealed, Society of Automotive Engineers, 1996
11. V. Nagpal, T.L Subramanian, and T.A. Altan, "ICAM Mathematical Modeling of Shear Metal Formability Indices and Sheet Metal Forming Processes", Technical Report AFML-TR-79-4168, AFML/LTC, Wright Patterson Air Force Base (WPAFB), 1979